RSC Advances

ROYAL SOCIETY OF CHEMISTRY

www.rsc.org/advances

RSC Advance

ARTICLE

Poly (vinylidene fluoride) / Poly (acrylonitrile)–based Superior Hydrophobic Piezoelectric Solid Derived by Aligned Carbon Nanotube in Electrospinning: Fabrication, the Phase Conversion and Surface Energy

Received 00th January 20xx,
Accepted 00th January 20xx

DOI: 10.1039/x0xx00000x

www.rsc.org/

Salem M. Aqeel [a,b], Zhe Wang [*a,c], Lisa Than [c], Gollapudi Sreenivasulu [d] and Xiangqun Zeng [*b]

Multifunctional materials have attracted many interests from both fundamental and practical aspects, such as field–effect transistor, electric protection, transducers and biosensor. Here we demonstrated the first superior hydrophobic piezoelectric surface based on the polymer blend of polyvinylidene fluoride (PVDF)–polyacrilonitrile (PAN) assisted with functionalized multiwalled nanotubes (MWNTs), by a modified electrospinning method. Typically the β–phase polyvinylidene fluoride (PVDF) was considered as the excellent piezoelectric and pyroelectric materials. However, polar β–phase of PVDF exhibited a natural high hydrophilicity. As a well–known fact, the wettability of the surface is dominated by two major factors: surface composition and surface roughness. The significant conversions derived by the incorporation of MWNTs, from nonpolar α–phase to highly polar β–phase of PVDF, were confirmed by FTIR. Meanwhile, the effects of MWNTs on the improvement of the roughness and the hydrophobicity of polymer blend were evaluated by atomic force microscopy (AFM) and contact angle (CA). Molar free energy of wetting of the polymer nanocomposite decreases with increasing the wt.% of MWNTs. All molar free energy of wetting of PVDF–PAN/MWNTs were negative, which means the non–wettability of film. The combination of surface roughness and low–surface–energy modification in nanostructured composites leads to high hydrophobicity. Particularly, fabrication of superior hydrophobic surfaces not only has fundamental interest but also various possible functional applications in micro– and nano–materials and devices.

1. INTRODUCTION

Poly-piezoelectric materials exhibit unique electronic performance comparable to those with silicon-based materials. Organic field-effect transistors (OFETs) are of great interest for applications in disposable electronic devices, such as radio-frequency identification tags, sensors application as well as in flexible-display device.[1, 2] A superior hydrophobic surface, especially superior hydrophobic piezoelectric solids, has attracted much interest from both fundamental and practical aspects, such as field–effect transistor, electric protection, transducers and biosensor.[3] The hydrophobicity will provide less interference from water which is major fail reason for electrical device especially for piezoelectric polymer. The high hydrophobicity surface could make organic semiconductor material more stable and bring wide applications for this material. Generally there are two basic strategies to increase the contact angle and formation of a more hydrophobic surface. One is to increase the surface roughness, which is known as the geometrical micro/nanostructure method. Another is modification of surface composition to lower surface energy.[4, 5] Current methods to prepare superior hydrophobic surface are based on the surface post modification[6, 7]. In recent years, many hydrophobic materials have been developed by using various components, such as polypropylene surfaces[8], poly(methyl methacrylate) and polystyrene[9] , polyurethane and poly(vinyl chloride)[10], with different techniques. It was found that the electrospinning are one of the attractive methods to alter the wetting behaviour of the polymer surface.[11, 12] A superior hydrophobic piezoelectric solid for wide applications are barely reported.

[a] Department of Chemistry, Faculty of Applied Science, Thamar University, P. O. Box 87246, Thamar, Yemen
[b] Department of Chemistry, Oakland University, Rochester, Michigan 48309, United States
[c] Chemistry Department, Xavier University of Louisiana, New Orleans, Louisiana, 70125, United States
[d] Physics Department, Oakland University, Rochester, Michigan, 48309, United States
See DOI: 10.1039/x0xx00000x

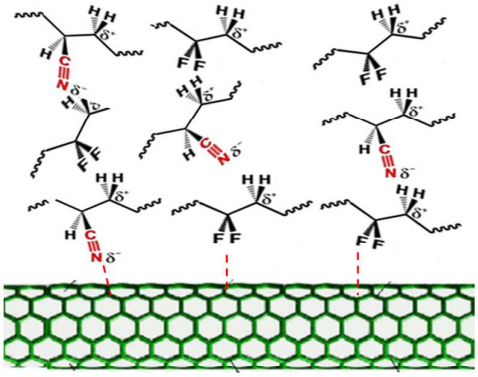

Scheme 1: Schematic representation of the PVDF–PAN interaction with MWNTs

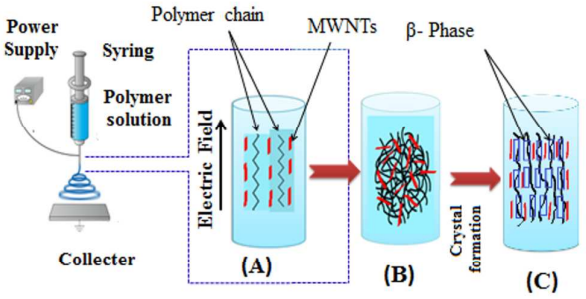

Scheme 2. Schematic diagram of the interaction between polymer blend (PVDF/PAN) and CNTs in the electrospinning. (A) the orientation of polymer blend (in black color) and MWNTs (in red color) under electric field, (B) the β-phase formation instead of the α-phase and (C) the β-crystal formation in PVDF for polymer nanocomposites (in blue color).

Polyvinylidene fluoride (PVDF) is a ferroelectric and piezoelectric polymer with excellent resistance to creep, fatigue and chemical attack, high mechanical and impact strength, after poling[13-15]. Thus it has been extensively studied for a broad range of applications, including, but not limited to, transducers [16], non–volatile memories [17], and electrical energy storage [18, 19]. As a typical semi–crystalline polymer, PVDF exists in five crystalline forms (α, β, γ, δ and ε–phases) [20]. Among the five polymorphs, β–phased PVDF (TTTT) exhibits outstanding piezoelectric and pyroelectric performance due to its highly polar structure compared to nonpolar α–phase (TGTG'), which is primary formation of PVDF. The variable approaches have been developed to achieve high β–phase formation PVDF in the last 30 years, such as, applying an extremely high electric field to the α–phase of PVDF,[21] and with optimized crystallization process from solution[22], from the melt[23], surface epitaxy[24], assisted with supercritical carbon dioxide method [25], and electrospinning method[26-29].

Another hand for superior hydrophobic PVDF films, there are several methods have been developed so far.[30, 31] However, superior hydrophobic piezoelectric PVDF coating method, which contains high β–phase content and increased contact angle, are barely reported. Currently some researchers indicated that the induction of nanomaterials could increase the surface roughness and also derive the α–phase of PVDF to β–crystal formation during a chain alignment caused by the electrostatic interaction between the methylene and charged nanoparticles[32-36]. The zigzag carbon atoms on the carbon nanotubes (CNTs) surface could induce β–phase formation during the crystallization of PVDF [37-39] and π conjugated structure of CNTs will attract the F- to CNTs surface. On another hand, CNTs could create a rough surface at mirco/nanometer level owing to their rigid cylindrical nanostructures with a diameter ranging from about 1 nm to dozens of nanometers and length ranging from hundreds of nanometers to micrometers[40]. And aligned CNTs could polymer structure could enhance Aligned Polyacrylonitrile Nanofibers.

The well–compatibility of PVDF with other polymers, attributed to the existence of quasi–hydrogen bonding between each other, provide the new approach to fabricate the composite structure by a copolymerization process, which could avoid the compromise made between the functionalization of CNTs and structure integrity in CNT–polymer composites. Polyacrylonitrile (PAN) is an ideal precursor for this purpose because it not only acted as a precursor for carbonaceous materials[41-45], –CN groups of PAN could build the intrachain and interchain interactions in the PVDF matrix via secondary bonding[46, 47].

In this work, carbon nanotubes were aligned in polymer matrix by the electrical field and mechanical force during an electrospinning process. And aligned CNTs were acted to nucleate and induce the PVDF chain on the CNTs surface via the electron–dipole interaction with CF_2 dipoles. PAN was blended in this composite to increase the compatibility of PVDF with CNTs (Scheme 1). Furthermore PAN could contribute the piezoelectricity of composite.[48, 49] There is no report on the preparation of PVDF/PAN with MWNTs nanocomposites. In this study, we hypothesize that by combination of the PVDF/PAN blends with MWNTs, of which has high surface ratio to volume that will effectively improve the piezoelectric and hydrophobic properties of polymer nanocomposites. It is believed that the nanostructure of the nanofibers and also their lower density contribute to the very large fraction of air in the surface, which is essential to the superior hydrophobicity.[50] The morphology, roughness, and hydrophobic properties of the resulting polymer nanocomposites (PVDF–PAN/MWNTs) were examined respectively. Fourier transforms infrared (FTIR) spectroscopy techniques allowed us to detect properties of the composites prepared as a function of the MWNTs content.

2. Experimental Section

PVDF with an average molecular weight of 275×10^3 g/mol and PAN with a molecular weight 150×10^3 g/mol were obtained from Sigma Aldrich co., dimethylformamide (DMF) form VWR International LLC. Functionalized multi-walled carbon nanotubes (MWNTs-COOH) were supplied by Nanostructured & Amorphous Materials, Inc., USA with diameter 10 nm, length 10–30 micron and content of –COOH 1.9-2.1 wt%.

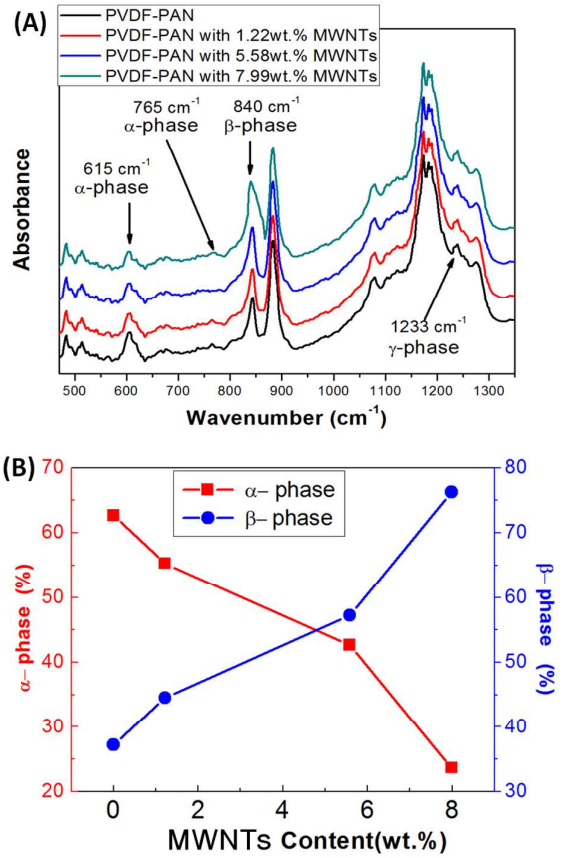

Figure 1: (A) FTIR spectra of PVDF–PAN and PVDF–PAN/MWNTs nanocomposites (B) plot of α, β–formation as a function of wt. % of MWNTs in PVDF–PAN/MWNTs nanocomposites.

The polymer blends were prepared by dissolving PVDF and PAN with polymer weight percentage ratio (50:50) in DMF at the polymer blend /solvent weight ratio of 20/80 under stirring for 2 hours at 70 ^{o}C. The MWNTs-COOH were dispersed with different weights in the PVDF-PAN solution via 30-min sonication followed by continuous stirring for 6 hours. The PVDF-PAN/MWNTs solutions were then placed in a plastic syringe fitted with a needle with a tip-diameter of 200 μm, and electrospun at 15 kV. A syringe pump was used to feed the polymer solution into the needle tip at flow rate of 2.5 mL/h and the distance between the needle tip and collecting plate was 10 cm (Scheme 2). The fiber was deposited on an Al sheet on the grounded electrodes, both as a flat sheet and on a rotating drum. All the electrospinning process was performed at 25 ^{o}C and humidity of 65%. All the samples were dried in vacuum at room temperature overnight prior to characterization. For the characterization of the samples, a Fourier transform infrared spectrometer, FTIR (Varian 3100, FTIR) was carried at room temperature. Each spectrum was recorded from 4000 to 400 cm^{-1} using 32 scans at a resolution of 4 cm^{-1}. The surface morphology of the PVDF-PAN/MWNTs was studied using an Atomic Force Microscope (Agilent Technology, Model N 9610 A). The surface images were recorded in the non-contact mode at different scan areas. The contact angle values of the samples were measured by sessile drop method using Contact Angle goniometer (Kyowa Interface Co. Ltd). The sessile drop was formed on the surface by depositing a droplet of deionized water slowly and steadily onto the membrane surface using a microsyringe. The contact angle was measured at room temperature. The value reported is the average of three measurements. The morphology, of the composite was characterized by scanning electron microscopy (SEM) (JSM-6510GS from JEOL), operating with an accelerating voltage of 20 kV.

3. Results and Discussion

The polyvinylidene fluoride (PVDF)–polyacrilonitrile (PAN) with functionalized multiwalled nanotubes (MWNTs) nanocomposites were characterized by multiple techniques including spectroscopy (FTIR), Microscopy (AFM) and contact angle measurements to correlate its surface energy with its morphology and surface tension. During the blending, the PVDF chains are very mobile and can effectively wrap over CNTs[51]. Their fluorine groups are strongly attracted by the delocalized π –electron clouds on the CNTs and can thus establish donor–acceptor complexes. In these complexes, the mobility of PVDF chains is limited due to the strong interaction between delocalized π –electron clouds on CNTs and electrophilic fluorine groups on the PVDF chains[52]. The FTIR spectra of the polymer nanocomposites were analyzed to confirm the interaction between polymer blends and MWNTs. In order to perform the quantitative measurement with FTIR, the high resolution transmission mode was used at same sample condition. FTIR system was stabilized with nitrogen liquid for 30mins. The peaks at 1180 cm^{-1} of C-F bond and 2214 cm^{-1} of C-N were use as standard. Figure S1 shows the FTIR spectra of PVDF–PAN/MWNTs. The FTIR spectra of MWNTs showed major peaks, located at 2880, 2361–2364, 1700 and 1560 cm^{-1}. The peak at 2880 and 2361–2364 cm^{-1}is attributed to H–C stretch modes of H–C=O in the carboxyl group and O–H stretch from strongly hydrogen–bonded –COOH respectively, while the peaks at 1700 and 1560 are corresponded to carbonyl groups of COOH and the C=C stretch of the COOH in MWNTs respectively. The characteristic peak at 2214 cm^{-1} is due to the stretching vibration of cyano group (–CN), 1454 cm^{-1} for (–CH_3) and 1373 cm^{-1} (–CH_2), which can be observed in PAN. On the other hand the spectra showed strong absorption band at 1140–1180 cm^{-1} (–CF_2 bending), and 1411–1419 cm^{-1} (–CH_2 stretching mode). The inset of Figure S1 demonstrates a small shift of the CN and CF_2 peaks following the MWNT embedding compared with the PVDF/PAN blend. The CN band, originally appearing at 2214 cm^{-1}, shifted slightly to 2227 cm^{-1} for the PVDF/PAN/MWNT composite; however, it was evident that the C-F peak for PVDF/PAN/MWNT (1156 cm^{-1}) shifted compared to the PVDF/PAN blend (1140 cm^{-1}).

As shown in Figure 1 (A), the characteristic peaks of the α–phase (non–polar phase) was obtained at 615, 765, and 790 cm^{-1}, while the characteristic peaks of the β –phase (polar phase) was observed at 510, 840 and 1270 cm^{-1}. The characteristic peaks of the γ phase were observed at 1233 cm^{-1}. The γ–phase can be obtained from strongly polar solvents such as DMF. In electrospinning, piezoelectric (β and γ) phases could still be induced via dipolar/hydrogen interactions between the local polar structure in the crystalline PAN and PVDF[53]. These results were similar to that reported for PVDF/nylon 11 blends [54]. The crystal structure of PVDF could be identified clearly from the FTIR results by using following equation[55].

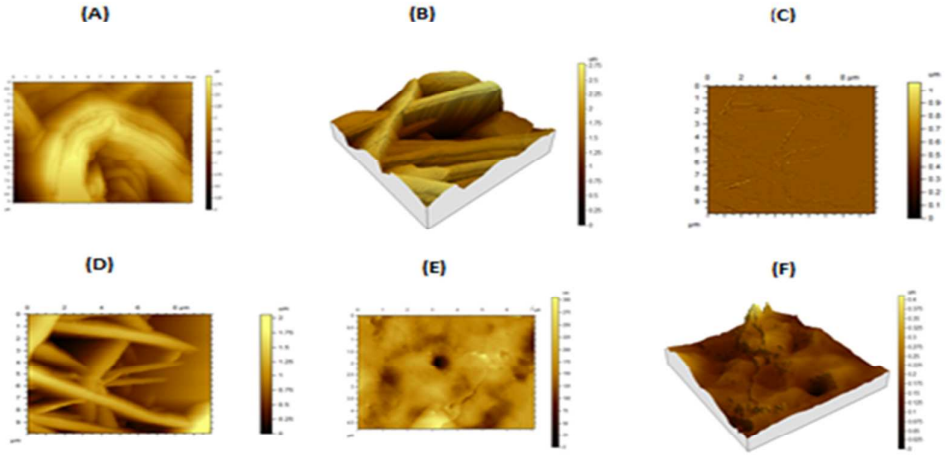

Figure 2A–F : AFM images of surface topography and three–dimensional surface for PVDF–PAN/MWNTs nanocomposites with (A)0 wt. % (B) 1.22 wt. % (C)5.58 wt. % (D) 5.58 wt. % (E) 7.99 wt. % and (F) 7.99 wt. %

$$F(\alpha) = \frac{A_\alpha}{A_\alpha + 0.8\, A_\beta} \quad (1)$$

and

$$F(\beta) = \frac{A_\beta}{1.26\, A_\alpha + A_\beta} \quad (2)$$

A_α and A_β correspond to the absorption bands of α–phase and β–phase respectively. The results were summarized in figure 1 (B). Opposite trends of these two crystal phases were observed with increasing of MWNTs concentration. The intensity of β–phase became stronger, while the bands of α–phase became weaker, suggesting the progressive conversion of α–phase by β–phase. Similar observations had been reported.[56, 57] It is well known that, the specific surface area of the MWNTs was higher than that of PVDF. With a higher specific surface area, the MWNTs can act as nucleating agents in the initial crystallization process of PVDF, which leads to a high degree of crystallinity.[58] However the mechanism of electromechanical coupling increasing is complicated. This mechanism is influenced by fluctuations in the electric field and anisotropy. The increasing the high polar β–phase content will change hydrophobic properties. Another hand a change in the constituent volume fraction was considered to lead to a competing change in mechanical and electrical properties too. It was reported that it could result a negative effect on the overall electromechanical coupling[59].

Under an external electric field in electrospinning, the conductive MWNTs can produce inductive charges on the surface, thus leading to a greater Coulomb force during the electrospinning processes. This attracts PVDF chains to crystallize partially on the MWNTs surface in the β–phase, but localized amorphous microstructures still exist (Scheme 2). With the electrostatic interaction of functional groups on the MWNTs (which then act as nucleating agents) with the polar–CF_2, the PVDF chain will have the zig–zag (TTTT conformation) of the β–phase, instead of the coiled α–phase (TGTG conformation). It is consistent with the results of β–crystal formation in PVDF/nanoclays composite.[37, 60, 61]

AFM is based on the interaction forces (short– or long–range, attractive or repulsive) that exist between atoms and molecules, and these forces are present on all materials. It provides quantitative, three–dimensional images and surface measurements with a spatial resolution of a few micrometres down to a few angstroms. The non–contact mode (NC–AFM) was considered as a more effective method than contact mode (C–AFM) in imaging small pores such as those in ultrafiltration and nanofiltration membranes. Because the diameter of the cantilever tip apex is greater than the pore diameter, while the tip is passed over the small pore, the tip cannot penetrate into the pore, and there will not be a great change in cantilever deflection.

Figure 2A–F represent selective AFM images of surface topography and a three–dimensional surface for PVDF–PAN/MWNTs composites. The full size images were presented in Figure S2. It was observed that the fibres of PVDF–PAN/MWNTs have nonwoven structures with fibre diameters about 400 nm and pore size diameter 480 nm. Functional groups in PAN of this nanocomposite lead to a strong interfacial bonding between the nanotubes and surrounding polymer chains to ensure the stability of the structuration of the surface during electrospinning, resulting in the infusible characters of PAN in the polymer nanocomposites.

Roughness parameters were obtained with the AFM analysis software. The average roughness (R_a) for the image is defined as the arithmetic average of the absolute values of the surface height deviations measured from the center plane. The root mean square roughness (R_q) represents the standard deviation from the mean surface plane. R_a and R_q seem to be most helpful and consistent in characterizing surface topography of the spun nanofiber.

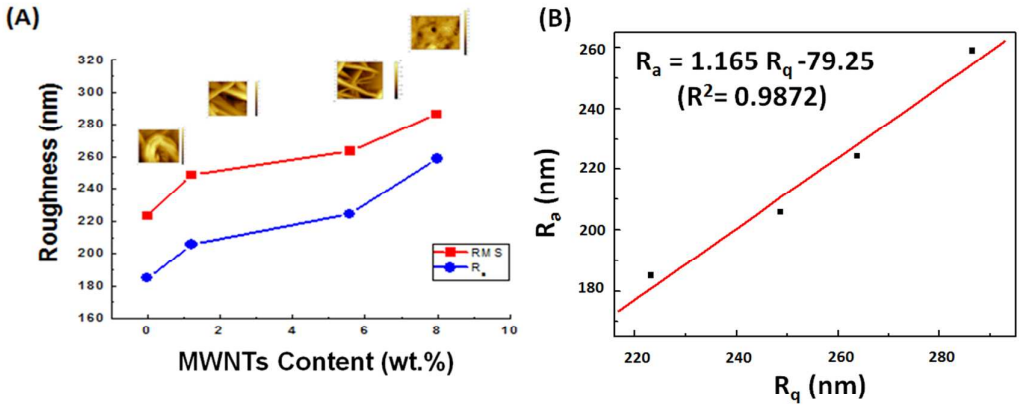

Figure 3: (A) The roughness of PVDF–PAN/MWNTs nanocomposites as a function of wt. % of MWNTs (B) Plot of R_a as a function with R_q of the PVDF–PAN/MWNTs nanocomposites.

As shown in Figure 3 (A) the pure PVDF–PAN presented the rough surface (R_a = 185 nm and R_q = 223.1 nm) and the roughness of PVDF–PAN/MWNTs increases as the MWNTs wt.% increases. The PVDF–PAN/MWNTs exhibited the roughest surface (R_a = 259 nm and R_q = 286.5 nm) with the increase of MWNTs content. Similar results were found where the roughness increased due to the combined effect of electrospinning process and the added MWNTs as nanocomposites.[62, 63] Electrospun nanocomposites are sometimes necessary in order to achieve superhydrophobic properties because the polymer is not intrinsically hydrophobic enough or does not make enough roughness to achieve water repellency [62].

The R_a values for all of the composites were always smaller than the R_q values. Figure 3(B) plots R_a values as a function with R_q of PVDF–PAN/MWNTs nanocomposites. The relationship between these two parameters is linear. This relation can be described in such that the population distributions of z_i coordinates that describe composites exhibiting some mathematical regularity that is not dependent on the range of the z variable. The SEM images of the PVDF/PAN/ MWNT-COOH composite were given in Fig. S3. The functionalization of MWNTs increases the compatibility with PVDF/PAN so as to improve the dispersion of MWNT in polymer nanocomposite. The fibers of PVDF-PAN/CNTs have nonwoven structure. They are interconnected with a large number in different sizes. The fibers of PVDF/PAN/CNTs are more interconnected as the wt.% of CNTs in the composite increases. The interconnected network morphology is expected to probable molecular level interactions between C–F (in PVDF) and –CN (in PAN). This kind of molecular interaction was considered to induce the phase mixing between PVDF and PAN.[64, 65]

Contact angle of the surfaces is measured using sessile drop observation. Figure 4 A–C shows a water droplet formed on the electrospun PVDF–PAN/MWNTs surface. The droplet was falling onto the surface of PVDF–PAN/MWNT form beads and roll off, which means that the surface was self–cleaning. Figure 4 (D) represents the effect of MWNTs on the advancing and receding contact angles of PVDF–PAN/MWNTs nanocomposites. The advancing contact angle increases from 83.25 ^{o} to 117.68^{o} and the receding contact angles increases from 88.19^{o} to 111.70^{o}, a high water contact angle, which indicates a superior hydrophobicity. It was shown that the hydrophobic properties increased by increasing the wt. % content of MWNTs. The hydrophobic properties improvement is due to the high ratio of surface area to volume of MWNTs, roughness, low surface energy of fluorinated polymers and electrospinning method[66-68]. Compared to those kinds of composites prepared via solvent evaporation method, the electrospinning method provided much higher contact angle

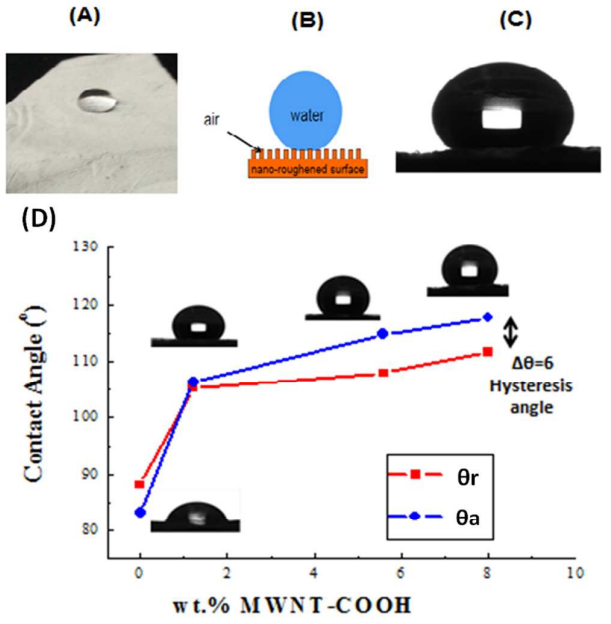

Figure 4: Photograph of (A) water droplets on the non–wettable, (B) graphical drawing of water droplet on nano–roughened surface and (C) contact angle of PVDF–PAN/MWNTs surface. (D) The advancing and receding contact angles of PVDF–PAN/MWNTs surface.

Table 1: Contact Angles, Wetting/Dewetting, Free Energies for PVDF–PAN/MWNTs composites.

MWNT (wt. %)	θ_a (deg)	θ_r (deg)	R_a (nm)	A (m^2/mol)	Δg_a (J/m^2)	Δg_r (J/m^2)	ΔG_a (J/mol)	ΔG_r (J/mol)	ΔG Hysteresis (J/mol)
0	83.25	88.19	185.0	10.11×10^{4}	-7.23×10^{-3}	-1.41×10^{-3}	−730.44	−142.55	-5.82×10^{-3}
1.22	106.36	105.27	205.7	9.78×10^{4}	-12.67×10^{-3}	0.26×10^{-3}	−1240.2	25.45	-12.93×10^{-3}
5.58	114.8	107.96	224.3	9.35×10^{4}	-17.73×10^{-3}	1.62×10^{-3}	−1658.8	151.61	-19.35×10^{-3}
7.99	117.68	111.71	259.0	9.07×10^{4}	-20.05×10^{-3}	1.42×10^{-3}	−1817.2	128.71	-21.47×10^{-3}

because of the high surface area of the formed fibers that ranges from nanometer to submicron scale[68].

Contact angle hysteresis (CAH), θ_H is typically defined as the difference between advancing contact angle, θ_a and receding contact angle, θ_r. It was found that the hysteresis increased by increasing the roughness. This effect can arise from molecular interactions between the liquid and solid or from surface anomalies, such as roughness or heterogeneities. The typical parameter used to characterize a solid surface wettability is the contact angle, which represented the angle formed between the liquid–solid and the liquid–vapor interfaces. The equations used to estimate free energies can be described as adsorption (or desorption). The surface free energy of wetting, Δg_a, is calculated as [69, 70]:

$$\Delta g_a = (1/3)(RT/A)\ln\left[(1-\cos\theta_a)^2(2+\cos\theta_a)/4\right] \quad (3)$$

For polymers, molar surface area A can be calculated assuming the surface is molecularly smooth and each molecular segment acts as an adsorption site. The area per site A site is taken as the 2/3 root of the volume of a single molecular segment V_{site}:

$$A_{site} = (V_{site})^{2/3} = (M/\rho N)^{2/3} \quad (4)$$

where ρ is the polymer density, M is molecular weight of the polymer repeat unit, and N is Avogadro's number. Multiplying Eq. (2) by Avogadro's number gives molar surface area A,

$$A = (M/\rho)^{2/3} N^{1/3} \quad (5)$$

The surface free energy of dewetting can be calculated as:

$$\Delta g_r = (RT/A)\ln(\theta_a/\theta_r) \quad (6)$$

Corresponding molar free energies, Δ*G*i, can be determined from molar surface areas,

$$\Delta G_i = A\,\Delta g_i \quad (7)$$

where *i* = a for an advancing contact line and *i* = r for a receding contact line, Δg_a is the surface free energy of wetting, Δg_r is the surface free energy of dewetting, A is the average molar area, of the polymer surfaces, M is the molecular weight of the polymer repeat unit, θ_a is the advancing contact angle, θ_r is the receding contact angle, θ_H is the contact angle hysteresis(CAH), ΔG_a is the molar free energy of wetting and ΔG_r is the molar free energy of dewetting. Table 1 lists the surface and molar wetting free energies of the various water/polymer–nanocomposites combinations. Δg_a unit is energy per area and is the change in the surface free energy of the solid due to wetting. Δg_a quantifies the strength of the interactions that drive spreading and lead to a liquid–solid bond.

All wetting free energies were negative, as expected from a spontaneous process, which means that the film is non–wettable and Δg_a decreases exponentially with an increase in θ_a. In contrast to Δg_a, Δg_r value is a measure of the energy required to initiate recession of the contact line. In this regard, dewetting energy is defined as a measurement of adhesion, which means the energy per area required to rupture a bond. Surface free energies of wetting and dewetting for the PVDF–PAN/MWNTs are plotted against MWNTs content in Figure 5 (A). Wetting free energies of the polymer nanocomposite decreases exponentially with increasing the wt.% of MWNTs. Surface free energy of dewetting, Δg_a of PVDF–PAN were negative, while surface free energies of dewetting for PVDF–PAN/MWNTs were positive. As Δg_a values, the magnitude of the free dewetting energies increased with increasing of MWNTs concentration. In other words, the energy to create the bond between the liquid and solid was equal to the energy to rupture it. However, dewetting free energies were positive when contact angle >90°. Values of measured contact angle can be strongly affected by the adding of MWNTs, which could have signigicant influence on the roughness of the measured surface. As the amount of MWNTs increased, the wettability of the films decreased due to the reduced surface energy and the enhanced roughness of nanocomposite.

All wetting free energies were negative, as expected from a spontaneous process, which means that the film is non–wettable and Δg_a decreases exponentially with an increase in θ_a. In contrast to Δg_a, Δg_r value is a measure of the energy required to initiate recession of the contact line. In this regard, dewetting energy is defined as a measurement of adhesion, which means the energy per area required to rupture a bond. Surface free energies of wetting and dewetting for the PVDF–PAN/MWNTs are plotted against MWNTs content in Figure 5 (A). Wetting free energies of the polymer nanocomposite decreases exponentially with increasing the wt.% of MWNTs. These energies have exponential trend in the decreasing

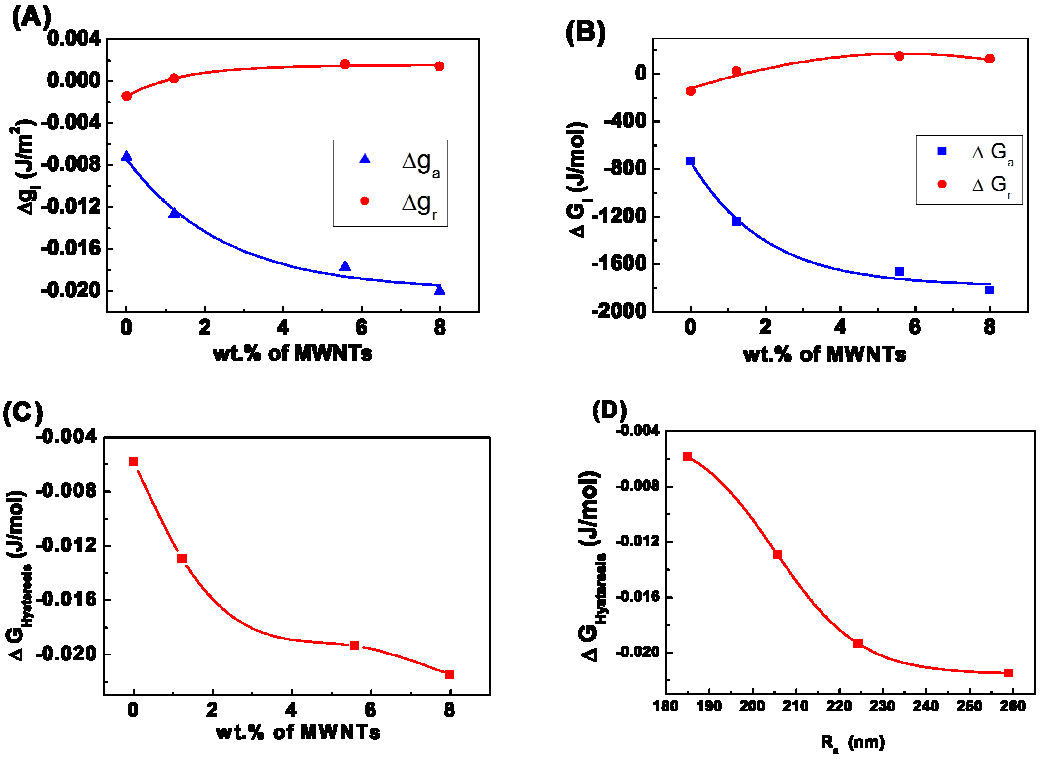

Figure 5: (A) Surface free energies of wetting / dewetting for the PVDF–PAN/MWNTs nanocomposite; (B) Molar free energies of wetting ΔGa and molar free energies of dewetting ΔGr for the PVDF–PAN/MWNTs nanocomposites; (C) The Hysteresis Molar free energies of PVDF–PAN/MWNTs nanocomposites; (D) The Hysteresis molar energies ΔGH of PVDF–PAN/MWNTs nanocomposites as a function of the roughness.

with increasing of the wt.% of MWNTs. However the content effect of carbon nanomaterials to surface roughness is complex and still investigating[71, 72].

Surface free energy of dewetting, Δg_a of PVDF–PAN were npiezoegative, while surface free energies of dewetting for PVDF–PAN/MWNTs were positive. As Δg_a values, the magnitude of the free dewetting energies increased with increasing of MWNTs concentration. In other words, the energy to create the bond between the liquid and solid was equal to the energy to rupture it. However, dewetting free energies were positive when contact angle >90°. Values of measured contact angle can be strongly affected by the adding of MWNTs, which could have signigicant influence on the roughness of the measured surface. As the amount of MWNTs increased, the wettability of the films decreased due to the reduced surface energy and the enhanced roughness of nanocomposite.

Molar free energies of wetting Δ*G*a and molar free energies of dewetting Δ*G*r for the PVDF–PAN/MWNTs are plotted against MWNTs content in Figure 5 (B). All molar free energy of wetting of PVDF–PAN/MWNTs were negative, which indicated the non–wettability of the film. The molar free energy of wetting of the polymer nanocomposite decreases with increasing wt.% of MWNTs. However molar free energy of dewetting of PVDF–PAN was negative, while the molar free energies of dewetting for PVDF–PAN/MWNTs were positive. The hysteresis molar free energy is the energy to create the bond between the liquid and solid and the energy to rupture it. The hysteresis molar energies, ΔG_H were negative and increases with an increasing wt.% of MWNTs (figure 5(C)). On the other hand, it was observed that the roughness influences the contact angle. As shown in figure 6(D)) the Hysteresis molar energies ΔG_H increases with increasing roughness, which means that the film is non–wettable (hydrophopic). Therefore, high hydrophobicity means not only a high roughness and high contact angle, but also a low hysteresis of the contact angle. The low hysteresis of the contact angle of the high hydrophobic surface is responsible for the self–cleaning properties, which means that a water droplet can easily roll off the surface and remove dust from the surface. The high hydrophobicity (non–wettable) properties of film can be useful for applications such as self–cleaning, anti–corrosion, anti–icing coating in aerospace industry and biofouling protecting.

4. Conclusion

High hydrophobic of PVDF–PAN/MWNTs nanocomposites with a wide composition range of MWNTs have been successfully prepared via electrospinning method. FTIR results indicated that MWNTs act as nucleation agent during crystallization and slightly increased the β–phase crystal and decreased the α–phase in the PVDF/ PAN/MWNTs nanocomposites. Since PVDF was considered as piezoelectric solid, the phase formation from nonpolar α–phase to highly polar β–phase could change PVDF piezoelectric properties. It was evident that the contact angle and surface roughness increased with increasing wt.% of MWNTs, which reduced the surface energy of film and the film is non–wettable. It can be concluded that the Incorporation of MWNTs into PVDF–PAN nanocomposites, plays a very important role in morphological and surface properties and the combination of surface roughness and low–surface–energy modification which leads to high hydrophobicity (non–wettable properties). The non–wettable properties of film can be useful for applications such as self–cleaning, anti–corrosion, anti–icing coating in aerospace industry and biofouling protecting.

Acknowledgements

Dr. Salem Aqeel acknowledges the Fulbright Scholar Program Advanced Research Award for a grant as postdoctoral research fellow. This research was done in Prof. Zeng's Research lab at Chemistry Department at Oakland University. Dr. Zhe Wang acknowledges NIH under Grant 2G12MD007595–06 for support. Author also thanks the NSF MRI Scanning probe microscope major instrument grant. Carolyn Le made editing work.

References

1. H. Yang, S. H. Kim, L. Yang, S. Y. Yang and C. E. Park, *Advanced Materials*, 2007, **19**, 2868-2872.
2. W. Liao, Z. Jia, Z. Guan, L. Wang, J. Yang, J. Fan, Z. Su and J. Zhou, *Dielectrics and Electrical Insulation, IEEE Transactions on*, 2007, **14**, 1446-1454.
3. P. Sista, M. P. Bhatt, A. R. McCary, H. Nguyen, J. Hao, M. C. Biewer and M. C. Stefan, *Journal of Polymer Science Part A: Polymer Chemistry*, 2011, **49**, 2292-2302.
4. S. K. Papadopoulou, C. Tsioptsias, A. Pavlou, K. Kaderides, S. Sotiriou and C. Panayiotou, *Colloids and Surfaces A: Physicochemical and Engineering Aspects*, 2011, **387**, 71-78.
5. M. S. Islam, N. Akter and M. R. Karim, *Colloids and Surfaces A: Physicochemical and Engineering Aspects*, 2010, **362**, 117-120.
6. M. T. Khorasani, H. Mirzadeh and Z. Kermani, *Applied Surface Science*, 2005, **242**, 339-345.
7. J. Zhang, J. Li and Y. Han, *Macromolecular Rapid Communications*, 2004, **25**, 1105-1108.
8. H. Y. Erbil, A. L. Demirel, Y. Avcı and O. Mert, *Science*, 2003, **299**, 1377-1380.
9. Y. C. Jung and B. Bhushan, *Nanotechnology*, 2006, **17**, 4970.
10. K. A. Mowery, M. H. Schoenfisch, J. E. Saavedra, L. K. Keefer and M. E. Meyerhoff, *Biomaterials*, 2000, **21**, 9-21.
11. M. Yue, B. Zhou, K. Jiao, X. Qian, Z. Xu, K. Teng, L. Zhao, J. Wang and Y. Jiao, *Applied Surface Science*, 2015, **327**, 93-99.
12. F. Huang, Q. Wang, Q. Wei, W. Gao, H. Shou and S. Jiang, *Express Polym. Lett*, 2010, **4**, 551-558.
13. M. Khayet, C. Y. Feng, K. C. Khulbe and T. Matsuura, *Polymer*, 2002, **43**, 3879-3890.
14. M. C. García-Payo, M. Essalhi and M. Khayet, *Journal of Membrane Science*, 2010, **347**, 209-219.
15. J.-U. Kim, S.-H. Park, H.-J. Choi, W.-K. Lee, J.-K. Lee and M.-R. Kim, *Solar Energy Materials and Solar Cells*, 2009, **93**, 803-807.
16. J.-C. Dubois, *Advanced Materials*, 1996, **8**, 542-542.
17. R. C. G. Naber, K. Asadi, P. W. M. Blom, D. M. de Leeuw and B. de Boer, *Advanced Materials*, 2010, **22**, 933-945.
18. B. Chu, X. Zhou, K. Ren, B. Neese, M. Lin, Q. Wang, F. Bauer and Q. M. Zhang, *Science*, 2006, **313**, 334-336.
19. F. Guan, J. Pan, J. Wang, Q. Wang and L. Zhu, *Macromolecules*, 2010, **43**, 384-392.
20. A. J. Lovinger, *Macromolecules*, 1982, **15**, 40-44.
21. J. Scheinbeim, C. Nakafuku, B. A. Newman and K. D. Pae, *Journal of Applied Physics*, 1979, **50**, 4399-4405.
22. R. L. Miller and J. Raisoni, *Journal of Polymer Science: Polymer Physics Edition*, 1976, **14**, 2325-2326.
23. A. J. Lovinger, *Polymer*, 1981, **22**, 412-413.
24. J. Wang, H. Li, J. Liu, Y. Duan, S. Jiang and S. Yan, *Journal of the American Chemical Society*, 2003, **125**, 1496-1497.
25. M. Imran-ul-haq, B. Tiersch and S. Beuermann, *Macromolecules*, 2008, **41**, 7453-7462.
26. M. Nasir, H. Matsumoto, T. Danno, M. Minagawa, T. Irisawa, M. Shioya and A. Tanioka, *Journal of Polymer Science Part B: Polymer Physics*, 2006, **44**, 779-786.
27. W. A. Yee, M. Kotaki, Y. Liu and X. Lu, *Polymer*, 2007, **48**, 512-521.
28. E. Öğüt, O. S. Yördem, Y. Z. Menceloğlu and M. Papila, 2007, pp. 65260Q-65260Q-65210.
29. J. Zheng, A. He, J. Li and C. C. Han, *Macromolecular Rapid Communications*, 2007, **28**, 2159-2162.
30. M. Peng, H. Li, L. Wu, Q. Zheng, Y. Chen and W. Gu, *Journal of Applied Polymer Science*, 2005, **98**, 1358-1363.
31. W. Zhang, Z. Shi, F. Zhang, X. Liu, J. Jin and L. Jiang, *Advanced Materials*, 2013, **25**, 2071-2076.
32. B. Luo, X. Wang, Y. Wang and L. Li, *Journal of Materials Chemistry A*, 2014, **2**, 510-519.
33. S. Garain, T. K. Sinha, P. Adhikary, K. Henkel, S. Sen, S. Ram, C. Sinha, D. Schmeißer and D. Mandal, *ACS Applied Materials & Interfaces*, 2015, **7**, 1298-1307.
34. B. N. Sahoo and K. Balasubramanian, *RSC Advances*, 2015, **5**, 6743-6751.
35. K. Vasundhara, B. P. Mandal and A. K. Tyagi, *RSC Advances*, 2015, **5**, 8591-8597.
36. S. Vidhate, J. Chung, V. Vaidyanathan and N. A. D'Souza, *Polym J*, 2010, **42**, 567-574.
37. N. Levi, R. Czerw, S. Xing, P. Iyer and D. L. Carroll, *Nano Letters*, 2004, **4**, 1267-1271.
38. S. Manna and A. K. Nandi, *The Journal of Physical Chemistry C*, 2007, **111**, 14670-14680.
39. S. Yu, W. Zheng, W. Yu, Y. Zhang, Q. Jiang and Z. Zhao, *Macromolecules*, 2009, **42**, 8870-8874.
40. T. Wu, Y. Pan and L. Li, *Colloids and Surfaces A: Physicochemical and Engineering Aspects*, 2011, **384**, 47-52.
41. H. Guo, M. L. Minus, S. Jagannathan and S. Kumar, *ACS Applied Materials & Interfaces*, 2010, **2**, 1331-1342.
42. J. Sutasinpromprae, S. Jitjaicham, M. Nithitanakul, C. Meechaisue and P. Supaphol, *Polymer International*, 2006, **55**, 825-833.

43. D. Li, Y. Wang and Y. Xia, *Nano Letters*, 2003, **3**, 1167-1171.
44. S. Jagannathan, H. G. Chae, R. Jain and S. Kumar, *Journal of Power Sources*, 2008, **185**, 676-684.
45. X. Shen, Y. Ji and J. Wang, *Journal of Applied Polymer Science*, 2008, **110**, 313-320.
46. D. Esrafilzadeh, R. Jalili and M. Morshed, *Journal of Applied Polymer Science*, 2008, **110**, 3014-3022.
47. T.-Y. Liu, W.-C. Lin, L.-Y. Huang, S.-Y. Chen and M.-C. Yang, *Polymers for Advanced Technologies*, 2005, **16**, 413-419.
48. Y. S. Jo, Y. Inoue, R. Chujo, K. Saito and S. Miyata, *Macromolecules*, 1985, **18**, 1850-1855.
49. H. Ueda and S. H. Carr, *Polym J*, 1984, **16**, 661-667.
50. L. Feng, S. Li, H. Li, J. Zhai, Y. Song, L. Jiang and D. Zhu, *Angewandte Chemie International Edition*, 2002, **41**, 1221-1223.
51. Z. Zhang, J. Zhang, P. Chen, B. Zhang, J. He and G.-H. Hu, *Carbon*, 2006, **44**, 692-698.
52. Z. Guo, E. Nilsson, M. Rigdahl and B. Hagström, *Journal of Applied Polymer Science*, 2013, **130**, 2603-2609.
53. G. Zhong, L. Zhang, R. Su, K. Wang, H. Fong and L. Zhu, *Polymer*, 2011, **52**, 2228-2237.
54. Q. Gao and J. I. Scheinbeim, *Macromolecules*, 2000, **33**, 7564-7572.
55. A. Salimi and A. A. Yousefi, *Journal of Polymer Science Part B: Polymer Physics*, 2004, **42**, 3487-3495.
56. R. Song, D. Yang and L. He, *J Mater Sci*, 2007, **42**, 8408-8417.
57. L. He, J. Sun, X. Wang, L. Yao, J. Li, R. Song, Y. Hao, Y. He and W. Huang, *Journal of Colloid and Interface Science*, 2011, **363**, 122-128.
58. S. P. Bao, G. D. Liang and S. C. Tjong, *Carbon*, 2011, **49**, 1758-1768.
59. S. Rudykh, A. Lewinstein, G. Uner and G. deBotton, *Applied Physics Letters*, 2013, **102**, 151905.
60. J. Buckley, P. Cebe, D. Cherdack, J. Crawford, B. S. Ince, M. Jenkins, J. Pan, M. Reveley, N. Washington and N. Wolchover, *Polymer*, 2006, **47**, 2411-2422.
61. Y. W. Nam, W. N. Kim, Y. H. Cho, D. W. Chae, G. H. Kim, S. P. Hong, S. S. Hwang and S. M. Hong, *Macromolecular Symposia*, 2007, **249-250**, 478-484.
62. V. A. Ganesh, A. S. Nair, H. K. Raut, T. T. Yuan Tan, C. He, S. Ramakrishna and J. Xu, *Journal of Materials Chemistry*, 2012, **22**, 18479-18485.
63. P. Roach, N. J. Shirtcliffe and M. I. Newton, *Soft Matter*, 2008, **4**, 224-240.
64. H. Dong, V. Nyame, A. G. MacDiarmid and W. E. Jones, *Journal of Polymer Science Part B: Polymer Physics*, 2004, **42**, 3934-3942.
65. A. I. Gopalan, P. Santhosh, K. M. Manesh, J. H. Nho, S. H. Kim, C.-G. Hwang and K.-P. Lee, *Journal of Membrane Science*, 2008, **325**, 683-690.
66. C. Feng, B. Shi, G. Li and Y. Wu, *Journal of Membrane Science*, 2004, **237**, 15-24.
67. Y.-J. Kim, C. H. Ahn and M. O. Choi, *European Polymer Journal*, 2010, **46**, 1957-1965.
68. Y. Chen and H. Kim, *Applied Surface Science*, 2009, **255**, 7073-7077.
69. C. W. Extrand, *Langmuir*, 2003, **19**, 3793-3796.
70. C. W. Extrand, *Langmuir*, 2004, **20**, 4017-4021.
71. Y. Zhou, F. Pervin, L. Lewis and S. Jeelani, *Materials Science and Engineering: A*, 2008, **475**, 157-165.
72. M. A. Rafiee, J. Rafiee, I. Srivastava, Z. Wang, H. Song, Z. Z. Yu and N. Koratkar, *small*, 2010, **6**, 179-183.